TECHNICAL PAPER



Flow boiling critical heat flux experiments for a microchannel at high mass velocities

Rhandrey Maestri¹ · Cristiano Bigonha Tibiriçá²

Received: 17 December 2024 / Accepted: 2 May 2025 / Published online: 31 May 2025 © The Author(s) 2025, corrected publication 2025

Abstract

Many flow boiling applications require high critical heat flux (CHF) levels, which can be obtained with high mass velocities and microchannel flow. At the same time, some situations require non-electrical conductive refrigerants as halogenated fluids with boiling points distinct from water. Most of the CHF experiments available in the literature for halogenated fluids are available at low mass velocities, $G < 2000 \text{ kg/m}^2 \text{ s}$, and therefore, correlations used to predict CHF should be validated at high mass flow conditions. In this work, CHF experimental data were obtained at high mass velocity for R134a at microscale conditions. The data were obtained in horizontal 1.0 and 1.1 mm inside diameter stainless-steel single tubes with 100 and 46 mm heating lengths and mass velocities from 3000 to 26426 kg/m² s. CHF of up to 2212 kW/m² was measured; the highest CHF value reported in the literature for a single uniformly heated tube with R134a. The parametric trends of CHF were ascertained relative to important flow and geometrical parameters, and the experimental data were compared against 10 CHF predictive methods. The results of the comparisons showed agreements with correlations in the order of 35% mean absolute error. A new correlation is developed, achieving a prediction error of 11.6%.

Keywords Critical heat flux · Experimental flow boiling · High heat flux · High mass velocities · Microchannels · R134a

1 Introduction

Boiling heat transfer is generally used in heat exchanger systems due to its high efficiency compared to single-phase heat transfer. A limiting criterion for using boiling heat transfer is generally the critical heat flux (CHF), which is defined as a sudden decrease in the boiling heat transfer coefficient between a heated surface and the working fluid due to an increase in surface temperature, heat flux or pressure change [1]. Achieving high levels of CHF is an important goal in the

Technical Editor: Guilherme Ribeiro.

Rhandrey Maestri r.maestri@hzdr.de

Cristiano Bigonha Tibiriçá bigonha@sc.usp.br

- Experimental Thermal Fluid Dynamics, Helmholtz-Zentrum Dresden-Rossendorf, Bautzner Landstraße, 400, 01328 Dresden, Saxony, Germany
- Heat Transfer Research Group, Department of Mechanical Engineering, São Carlos School of Engineering, University of São Paulo, Avenida Trabalhador São-Carlense, 400, São Carlos, São Paulo 13566-590, Brazil

design of cooling devices such as diverters of fusion reactors [2], concentration photovoltaic [3], power transmission systems [4] and electric vehicles [5].

If the surface heat flux is increased above the CHF, the surface temperature will jump to the next stable operating point in the film boiling region [6]. In many practical cases, this significant temperature jump is enough to cause the heating surface to fail; hence, the colloquial name, burnout, often used to refer to this phenomenon [7-10]. Several factors affect the CHF flow boiling value, such as channel shape, fluid properties, heated tube length/diameter ratio, inlet vapor quality and velocity, among others [11]. One of the themes that draw attention from the researchers is the CHF enhancement, which can be achieved in distinct ways, such as modifications in surface [12, 13], length, diameter [14], fluids, nanoparticles addition [15, 16], changes in gravity [17] and instabilities suppression [11, 18]. Passive cooling techniques provide a means to reduce the system size and have been the subject of extensive studies, particularly in surface modifications or the use of nanofluids, both of which are promising for electronic cooling [19]. However, these passive techniques generally offer lower cooling capabilities



compared to active techniques, such as flow boiling, which can better manage heat dissipation under high thermal loads.

Only a few experimental CHF studies on high levels of CHF have been published, mainly for water flow. These investigations demonstrated that the highest levels of CHF can be achieved with the subcooled type of CHF, high mass velocities in small diameter, short length tubes and water as a working fluid [10]. But organic refrigerants, including halogenated ones like R134a, have gained renewed importance due to organic power cycles (ORC), a promising technology for utilizing renewable energy and industrial waste heat [20]. In addition to the constant miniaturization of the systems over the years [21], there is also a need to reduce the size of heat exchangers by using microchannels for the ORC applications. The application of organic fluids for power generation brought new requirements for these refrigerants that were typically used only in refrigeration applications. One of these aspects is the need for higher CHF values to become feasible using the most compact heat exchangers to reuse waste heat.

R134a is one of the most used refrigerants in history [22] and is a reference for new refrigerants that are being proposed. Due to the Kigali Amendment [23, 24] of Montreal protocol, which imposes restrictions on the use of high global warming potential (GWP) hydrofluorocarbons (HFC) refrigerants, R134a should be replaced all over the world by the end of 2040. New environmentally friendly refrigerants with low GWP values are being developed. Still, they should have better thermal performance than previously high GWP refrigerants to avoid more indirect gas emissions that would cancel their lower GWP benefits.

Table 1 compiles experimental studies of saturated and subcooled CHF using the fluid R134a. It shows that the maximum CHF value achieved in convective boiling, considering both single and multi-microchannels with different geometries, has a value of 1.0 MW/m^2 and the maximum flow rate (*G*) used in these experiments was $6000 \text{ kg/m}^2\text{s}$.

The symbols d and L_h are, respectively, hydraulic diameter and heated length. It is important to note that some experiments, such as Mauro et al. [25], reported CHF values greater than 3 MW/m², but such values were obtained using the heat exchanger base area; therefore, the CHF becomes 0.79 MW/m² when using the internal channel surface area dimension.

Considering this context, this paper presents new experimental data for CHF at high mass velocities for d=1.0 and 1.1 mm horizontal stainless-steel single tubes, which are still within the threshold diameter—at which microscale effects remain significant in a tube [34, 35]. Tests were conducted with R134a for heated lengths of 100 and 46 mm, and the experimental results were compared against predictive methods from the literature. These data are important to serve as a reference for comparison against future data of new low GWP refrigerants expected to substitute R134a.

2 Methodology

This section presents the experimental apparatus and provides an overview of the testing circuit. It describes the use of two distinct testing sections and specific details regarding temperature and pressure measurements. Later, the methodology used for measuring the critical heat flux (CHF) is detailed. Furthermore, the range of experimental parameters associated with this procedure will be systematically outlined.

2.1 Experimental apparatus

The experimental setup consists of refrigerant and water circuits. In the refrigerant circuit (Fig. 1), starting from the condenser, the test fluid flows through the filter, passing by a Coriolis mass flow meter (Optimass 6400, Krohne, Germany) to the pump. A bypass piping line containing a needle

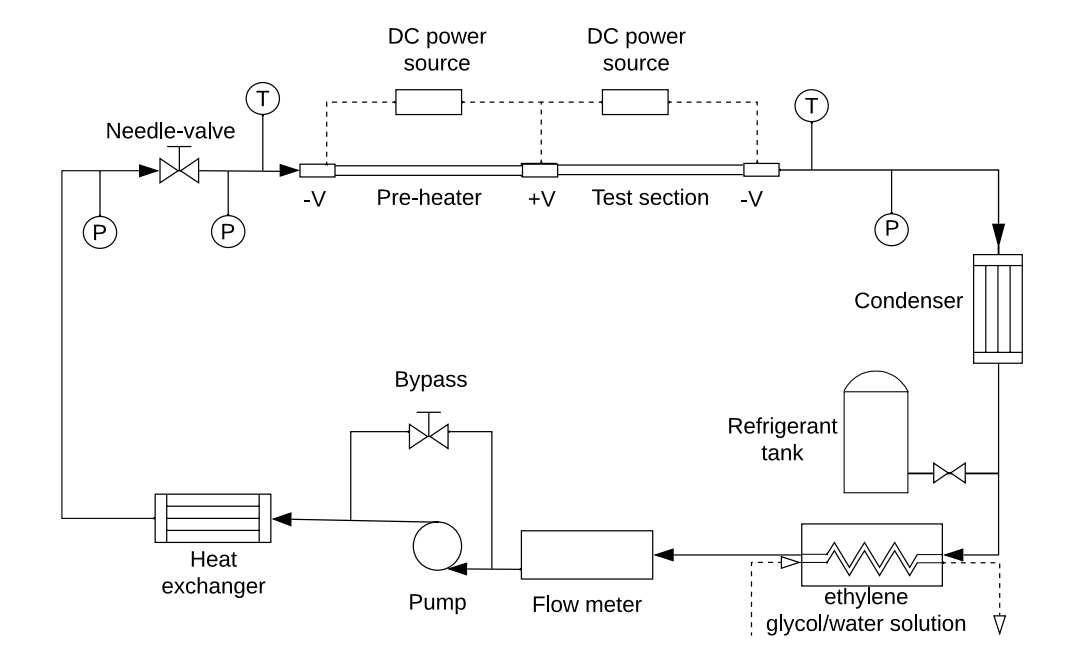
Table 1 Experimental studies from the literature involving CHF with R134a in convective boiling. Experiments involve different channel geometries, small channels $d \lesssim 10$ mm, a broad range of heated length L_h and the mass velocity G in which the highest CHF was achieved

Author	Geometry/number of channels	d (mm)	L_h (mm)	G (kg/m ² s)	CHF* (MW/m ²)
Wojtan et al. [26]	Circular/1	0.8	20	500	0.6
Mauro et al. [25]	Rectangular/29	0.315	30	1250	0.79
Ali and Palm [27]	Circular/1	1.22	220	600	0.16
Del and Bortolin [28]	Circular/1	0.96	97.5	500	0.142
Mikielewicz et al. [29]	Circular/1	1.15-2.3	385	700	0.220
Anwar et al. [30]	Circular/1	1.6	213	600	0.133
Song and Chang [1]	Circular/1	10.4	1000	6000	0.45
Mastrullo et al. [31]	Rectangular/7	1.33	35	350.5	1.0
Tan et al. [32]	Helical/1	9.7	3780	2095	0.45
Dalkılıç et al. [33]	Rectangular/27	0.421	40	1200	0.5

^{*}CHF values are based on the internal surface area of the channels



Fig. 1 Schematic diagram of the testing circuit. The arrow indicates the flowing direction of the fluids. P, T and V are, respectively, the positions of the pressure transducers, thermocouples and electrodes



valve is installed downstream of the pump so that the desired liquid flow rate (G) can be set with a frequency controller on the pump. Just upstream of the preheater inlet, the enthalpy (h_{in}) of the liquid is estimated from its temperature (T) by a thermocouple located at an adiabatic position on the outside tube wall and its pressure (P) by an absolute pressure transducer. In the reservoir (refrigerant tank), fluid is heated to the desired saturation pressure. The test sections are thermally insulated horizontal stainless-steel tubes and are heated by applying direct current (DC) to their surface. Once the liquid leaves the test section, a thermocouple on the external tube surface determines its temperature. A tubein-tube type heat exchanger with ethylene glycol/water solution is installed after the condenser to induce subcooling in the fluid prior to passing through the pump. For more details and a real photograph of the experimental bench, please refer to the previous publication [36].

In this work, test sections with two different lengths were used independently in different experiments. The first, schematically illustrated in Fig. 2, has a heated length of 100 mm. The second, shown in Fig. 3, has a heated length of 46 mm and was used to obtain higher levels of CHF. The sections consist of two types of AISI 304 stainless-steel tubes. The first tube is welded with a diameter of d = 1.0 mm and a wall thickness of 0.2 mm, while the second tube is seamless steel with a diameter of 1.1 mm and a wall thickness of 0.3 mm. To have better control of the inlet vapor quality (x_{in}) , a preheating (ph) section with a length of 49.5 mm between electrodes was used, as indicated in Fig. 3. The test sections with heated lengths of 46 and 100 mm have, respectively, 4 and 6 thermocouples installed on their surface. The temperatures are used to detect wall temperatures and CHF occurrence. The thermocouple (T6) was installed close to the output electrode to ensure the integrity of the tube in case of operation in conditions close to the critical heat flux.

2.2 Data reduction

In this section, we show the procedure used to obtain the relevant variables in this study: mass velocity, vapor quality and critical heat flux. The mass velocity is given by the ratio between the mass flow rate (\dot{m}) , measured by the

Fig. 2 Test section details when heated length $L_h = 100$ mm. The positions of each thermocouple (T) are indicated, and millimeter-long dimensions are indicated above each sector. T0 and T7 indicate, respectively, subcooling and saturation temperature. The flow direction is indicated from left to right. Electrode positions (-, +) are also indicated

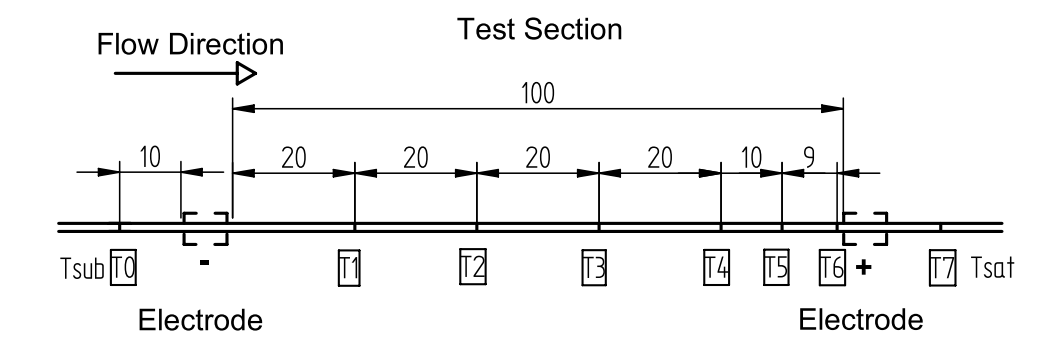
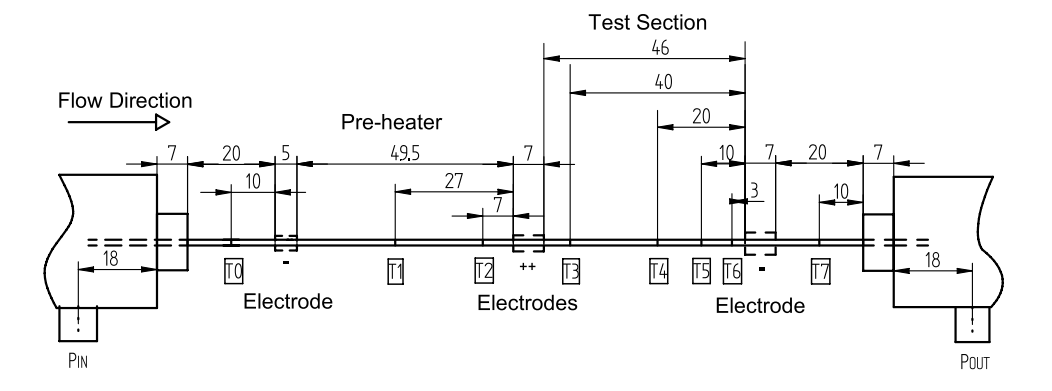




Fig. 3 Test section details when heated length L_h = 46 mm. T0 to T7 are thermocouples positions on the preheater and test sections. The flow direction is indicated from left to right. Electrode positions (-,++) are also indicated. Further details are indicated until $P_{\rm in}$ and $P_{\rm out}$, which are, respectively, the inlet and outlet absolute pressure transducer positions



Coriolis meter and the internal area of the tube cross section, $A_{\text{int}} = \pi \cdot d^2/4$, as shown in Eq. 1.

$$G = \frac{4 \cdot \dot{m}}{\pi \cdot d^2} \tag{1}$$

The vapor quality at the preheater or test section inlet (x_{in}) , as well as at the test section outlet (x_{out}) , is determined by an energy balance, Eq. 2:

$$x(z) = \frac{1}{h_{\text{lv}}(z)} \cdot \left[\frac{Q_{\text{ts}}(z) + Q_{\text{ph}}}{G \cdot A_{\text{int}}} + h_{\text{in}} - h_l(z) \right]$$
 (2)

where $h_{\rm lv}$, $h_{\rm in}$ and h_l are, respectively, enthalpies of vaporization, inlet and saturated liquid. The saturated liquid at the respective temperature position (z) can reasonably approximate each enthalpy.

The critical heat flux (CHF) is the ratio between the electrical power applied to the test section $(Q_{\rm ts})$ and the inner surface area of the tube, considering only the heated region, Eq. 3:

$$CHF = \frac{Q_{ts}}{\pi \cdot d \cdot L_h} \tag{3}$$

Electrical power on the test section is directly calculated by the product of voltage (V) and electrical current (i) provided by the DC power sources, $Q_{\rm ts} = V \cdot i$. For calculation purposes, it is considered that the heat flux is uniform along the tube and that heat losses to the environment in the heated region of the tube are minimum.

2.3 Experimental procedure

Initially, the refrigerant in the tank is heated by exchanging heat with water circulating in an external hose attached to the tank surface. The water exchanges heat with a thermostatic bath, allowing subsequent cooling to collect fluid from the experimental apparatus. In this way, the fluid pressure (*P*) in the main circuit is established from the pressure of the refrigerant in the tank, which is in a saturated state. Next, the mass flow rate (*m*) is imposed through the frequency inverter

acting on the pump. Thus, the subcooling temperature $(T_{\rm sub})$ of the fluid at the inlet of the preheater is adjusted through the flow of water in the heat exchanger located upstream of this section. Afterward, electrical power is applied, whether to the preheater $(Q_{\rm ph})$ in order to obtain the desired vapor quality at the test section inlet $(x_{\rm in})$ or direct to the test section $(Q_{\rm ts})$. The heat flux imposed on the preheater $(q_{\rm ph})$ or in the test section $(q_{\rm ts})$ is calculated in real-time through the LabVIEW program, allowing the adjustment of the test conditions. In this way, we can easily adjust the saturation temperature $(T_{\rm sat})$, mass velocity (G), heat flux (q) and vapor quality (x). Experimental data are recorded after verification of steady state, characterized by fluctuations in temperature measurements in the test section lower than the uncertainty of its measurements.

To measure the CHF, the power applied in the test section is increased in small steps. An effort was made to keep the remaining parameters under control. The CHF was defined when the wall temperature, measured by any of the thermocouples on the test section, reached 45 K of superheat. Usually, the thermocouple at the end of the test section (T6) was the first to reach this level. To illustrate the procedure, a curve of wall superheat $(\Delta T_{\text{sup}} = T(z) - T_{\text{sat}})$ where T(z) = T6) versus heat flux (q) during convective boiling, with a mass velocity of 3000 kg/m² s is shown in Fig. 4. In lower heat flux levels $0 \le q \le 75 \text{ kW/m}^2$, when the wall superheat is not high enough, R134a is in a singlephase liquid state. In this stage, a linear trend exists from 0 $\leq \Delta T_{\text{sup}} \leq 12 \text{ K.}$ After that, the onset of boiling promotes a slight decrease in the wall superheat, and a faster superheat of the surface follows with small increments of the heat flux. Before CHF occurrence, the wall superheat is smaller than 25 K. Above $q = 750 \text{ kW/m}^2$, a slight increase in heat flux causes a drastic increase in wall superheat. The superheat of 45 K resulted in a critical heat flux q = CHF = 767 kW/m². After that, the system rapidly deactivates the DC power source.

For the experimental campaign involving critical heat flux, the following experimental parameters were tested: tube manufacturing type, inner diameter (d), heated length



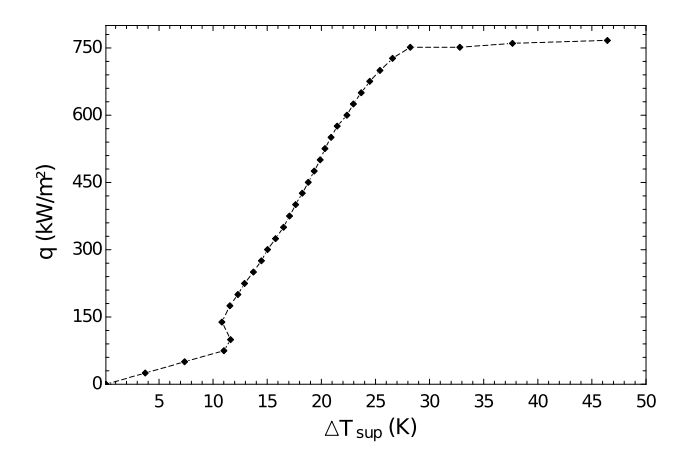


Fig. 4 Flow boiling curve in a microchannel with inside diameter d =1.1 mm, representing the heat flux (q) against wall superheat (ΔT_{sup}). The working fluid is R134a and mass velocity $G = 3000 \text{ kg/m}^2 \text{ s}$. Other operational parameters are constant as $T_{\rm sat} = 23$ °C, $\Delta T_{\rm sub} =$ 6 K and $L_h = 46 \text{ mm}$

 (L_h) , mass velocity (G), saturation temperature (T_{sat}) and inlet vapor quality (x_{in}) . Table 2 presents the range of these test conditions, along with the calculated outlet vapor quality (x_{out}) and critical heat flux (CHF).

2.4 Experimental uncertainties and validation of the experimental apparatus

Considering the need to ensure the quality of measurements, thus validating the results presented in this work, the uncertainties of the measured and estimated parameters are shown in Table 3. Uncertainty of the measuring instruments was used according to the technical specifications and calibration certificates of each equipment. In this study, the uncertainty of the temperature measurement was determined according to the calculation procedure proposed by Abernathy et al. [37]. The equations used to determine the uncertainty of each variable, following Moffat [38], are provided in the supplementary material (Sect. 1).

To ensure the accuracy of the vapor quality estimation and to assess the effective heat transfer rate for the fluid, a liquid phase energy balance ($\Delta E/E$) was performed based on Eq. 4:

Table 3 Uncertainty of measured parameters

Parameter	Uncertainty	Parameter	Uncertainty
d	20 μm	P	0.5 kPa
L_h	1.0 mm	$Q_{\mathrm{ts}},Q_{\mathrm{ph}}$	1%
G	2%	T	0.15 °C
CHF	< 6%	x	< 10%

$$\left(\frac{\Delta E}{E}\right) = \frac{\left[\left(\frac{\pi d^2}{4}\right)G(h_{\text{out}} - h_{\text{in}})\right] - (Q_{\text{ph}} + Q_{\text{ts}})}{Q_{\text{ph}} + Q_{\text{ts}}} \cdot 100 \tag{4}$$

This equation represents the increase in energy (E) due to the enthalpy difference $(h_{out} - h_{in})$ in response to the introduced heat $Q_{\rm ph}$ and $Q_{\rm ts}$. Figure 5 shows Eq. 4 with our experimental results against the Reynolds number (Re):

$$Re = \frac{G \cdot d}{u} \tag{5}$$

Most points are between \pm 5% of heat losses. Even though higher losses occurred for the tube with a 1.0 mm inside diameter and when using a preheater. For convective flow boiling experiments with high values of Reynolds number (Re), as in the case of the CHF tests, the internal heat transfer is much higher than the heat transfer in single-phase flow, lowering the heat losses to the environment.

3 Results

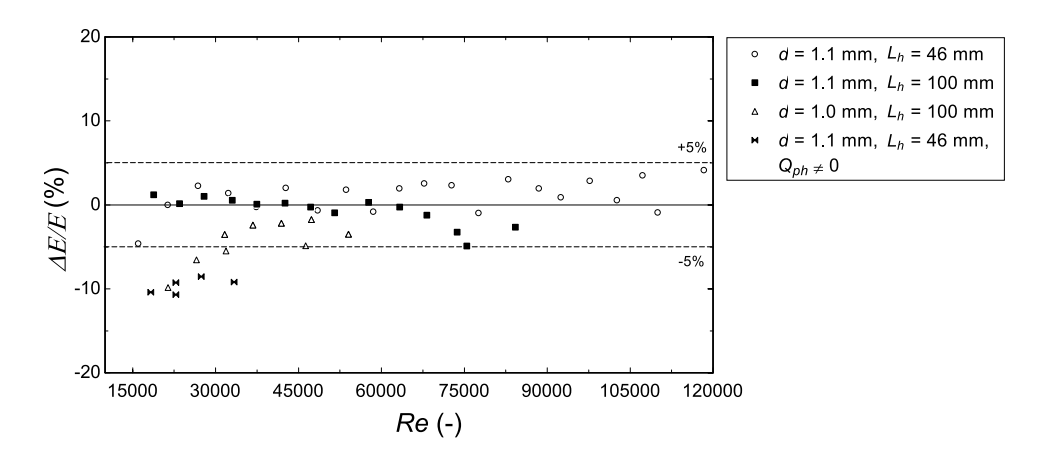
The calculated CHF and corresponding experimental conditions for each test are conveniently shown in Tab. S1 of the supplementary material (See Sect. 4). A total of 160 data points were acquired, with tubes of heating lengths L_h = 46.0 mm and 100 mm, inside diameters d = 1.0 mm and 1.1 mm. The main parameter we focused on was the mass velocity (G) due to its important effect on increasing the critical heat flux. Other parameters that have an effect on the flow boiling and critical heat flux were also included, such as saturation temperature $(T_{\rm sat})$, inlet subcooling $(\Delta T_{\rm sub})$, pressure drop in the valve that precedes the test section (ΔP_{valv}) together with inlet (x_{in}) and outlet vapor quality (x_{out}) . Except for points 99 to 151, where the preheating section

Table 2 Range of experimental parameters employed in this study considering two test sections with d = 1.0 and 1.1 mm. The calculated values of x_{out} and CHF are also indicated. R134a is the working fluid

d (mm)	L_h (mm)	G (kg/m ² s)	T_{sat} (°C)	<i>x</i> _{in} (-)	<i>x</i> _{out} (-)	CHF (kW/m ²)
1.0	100	6000-10000	32–36	-0.22 to -0.14	-0.05 to 0.07	515–652
1.1	100	3000-15000	27-39	-0.52 to -0.05	-0.31 to 0.41	136-1800
	46	3000-26426	25–33	-0.41 to 0.07	-0.32 to 0.23	613–2212



Fig. 5 Single-phase energy balance ($\Delta E/E$) calculated with Eq. 4 against Reynolds number (Re) for R134a. Dashed lines represent the error band of \pm 5. Different symbols represent the distinct configurations of the test section



with length $L_{\rm ph}=49.5$ mm was used, all other tests were performed with $L_{\rm ph}=0$. Notably, at line 160 with a mass velocity of G=26426 kg/m²s, the CHF reached 2212.00 kW/m², representing the highest experimental data for flow boiling of R134a in a single smooth microchannel, to the best of the author's knowledge.

Based on the data in Tab S1, in the next section, we present the relevance of the physical variables, evaluated with our experimental apparatus, when applying critical heat flux with high values of mass velocity (G) with R134a in a single microchannel. Some parametric effects will be analyzed, and predictive methods will be tested. In some analyses, we normalize the data based on the dimensionless numbers that have critical heat flux (CHF) or mass velocity (G) in its terms. They are, respectively, boiling number (Bo) and Weber number (We_d) , as shown, respectively, in Eqs. 6 and (7).

$$Bo = \frac{\text{CHF}}{G \cdot h_{\text{lv}}} \tag{6}$$

$$We_d = G^2 \cdot \frac{d}{\sigma \cdot \rho_l} \tag{7}$$

In our experiments, the mass velocity ranges from G = 3000 to $26420 \text{ kg/m}^2\text{s}$ and the CHF from 158.21 to 2212.00 kW/m², leading, respectively, to We = 1063 to 97633 and Bo = 0.000315 to 0.0004841.

3.1 Tube effect

One of the objectives of this study was the evaluation of the effect of the two types of AISI 304 stainless-steel tubes (1.0 mm welded tube and 1.1 mm seamless tube) in the CHF. Since the seam can change the local surface characteristics of the tube, it can be inferred that the seam could affect the CHF. Since both the welded and the seamless tubes have slightly different internal diameters, a direct comparison of their CHF values may give incorrect conclusions. To address

this issue, the CHF results (CHF_{exp}) for both tubes were compared against the CHF correlation (CHF_{the}) from Wojtan and Thome [26] in Fig. 6.

The dimensionless number $\eta = 1 - \text{CHF}_{\text{exp}}/\text{CHF}_{\text{the}}$ is plotted against the mass velocity (*G*). One can observe that η is between the \pm 10% error range in both tubes. When considering the welded tube (d = 1.0 mm), there is a mean absolute error (MAE) of 8.14% about Wojtan and Thome [26] CHF correlation while for the seamless tube an MAE of 7.16%. When analyzing the CHF behavior in AISI 304 stainless-steel tubes, it is evident that a seam did not seem to impact the CHF for the tested tubes substantially. Under similar conditions, both tubes exhibited similar CHF, indicating a notable stability in CHF values. This consistency suggests that, for the evaluated diameters and materials, the presence of a seam in the welded tube did not significantly affect the critical heat flux compared to the seamless tube.

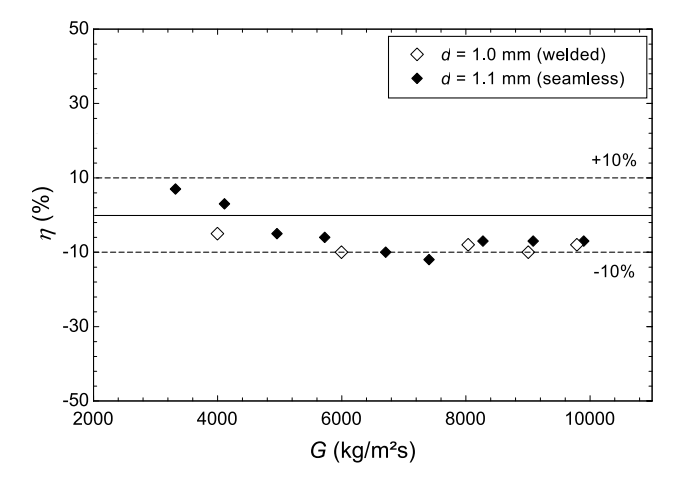


Fig. 6 The dimensionless number $\eta = 1 - \text{CHF}_{\text{exp}}/\text{CHF}_{\text{the}}$ is plotted against the mass velocity (*G*) for two types of tubes (welded and seamless with d = 1.0 mm and 1.1 mm, respectively)



Therefore, we continue our analysis considering only the seamless tube with an inside diameter of 1.1 mm.

3.2 Needle-valve effect

Previous works of one of the authors of this study have shown that the pressure drop on the valve (ΔP_{valv}), which precedes the test section, has a significant effect on the critical heat flux [11, 39]. Evidence suggests that carefully setting the pressure drop on that valve (ΔP_{valv}) can lead to a reduction of oscillations and reversible flow [11]. The reversal flow is caused by forces originating from bubble nucleation and its growth, which are sources of flow instabilities in the microchannels. Tibiriçá and Ribatski [39] show the time sequence on the position of the onset of nucleate boiling during a heat flux step increment with a low mass velocity of $G = 200 \text{ kg/m}^2 \text{s}$ where it is possible to see the reversal flow which can be prevented with a high-pressure drop.

Looking for an ideal scenario that can lead to the highest critical heat flux and a pressure drop that does not damage the experimental setup, we plot in Fig. 7a the effect of closing the needle-valve $(n_{\rm ph})$, located upstream of the preheater, for different bypass needle-valve (n_{RP}) adjustments on the CHF. In this experiment, the mass velocity is constant in $G \approx 4000 \text{ kg/m}^2\text{s}$. In the x-axis, the value of $n_{\text{ph}} = 0$ (zero) represents the valve completely closed, and $n_{\rm ph} = 50\%$ means the valve is half opened. The pressure drop curve (ΔP_{valv}) illustrated in Fig. 7b was obtained through the difference between readings of the absolute pressure transducers at the inlet of the test section and the pump outlet (see Fig. 1).

Tests were performed by first setting the bypass (BP) valve opening in $n_{BP} = 25$, 12.5, 6.25% and also completely closed, or $n_{BP} = 0\%$ of the opening. We measure the CHF and the inlet valve pressure drop in each BP opening for

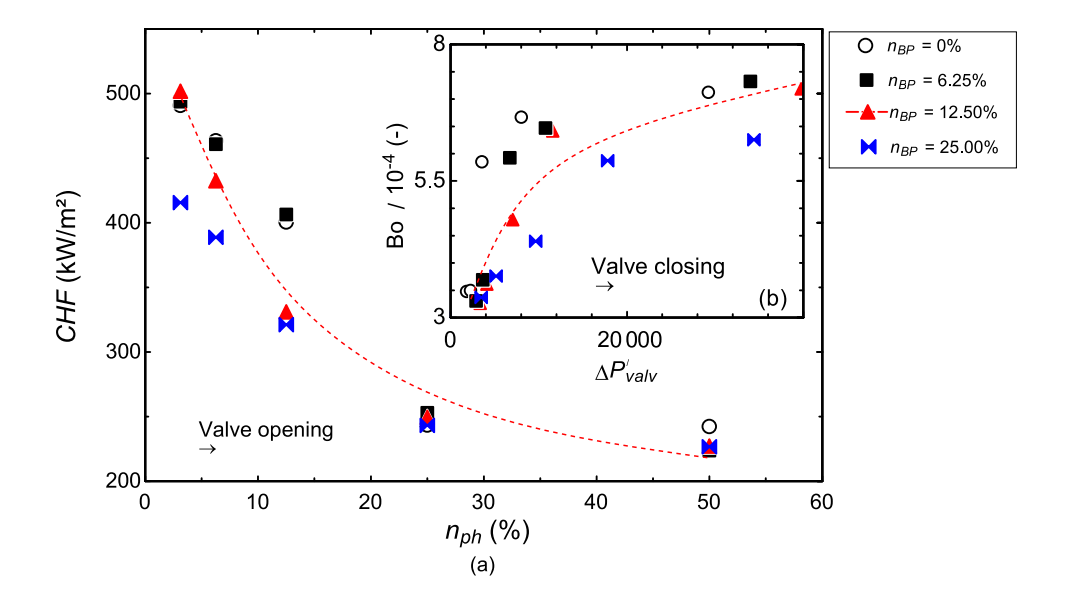
different values of preheater inlet valve turns. According to Fig. 7a, by decreasing the preheater valve opening $n_{\rm ph}$ from 50 to 3.125%, the CHF increases more than 100% for any bypass valve opening (n_{RP}) . As observed by the curve, the CHF in function of the preheater valve opening $n_{\rm ph}$ follows a trend defined by 175, 294.98 $\cdot n_{\rm ph}^{-0.31}$. The increase in the CHF is followed by an increase in the pressure drop in the valve ΔP_{valv} from approximately 100 to 500 kPa. Also, when opening the preheater valve $n_{\rm ph}$ by more than a quarter of a turn (25%), the CHF does not vary considerably regardless of the bypass valve n_{BP} . For all preheater valve opening values, there is an almost imperceptible difference when using the completely closed bypass valve about the 6.25% opening of the bypass valve. When bypass valve opening $n_{RP} >$ 6.25%, the CHF has a considerable influence. This can be related to the flow stability caused by the specific configuration of the pump rotation speed and curve, which the bypass affects. A logarithm curve relating the pressure drop in the valve ΔP_{valv} with the Bond number is shown in Fig. 7b, which is given by Eq. 8:

Bo =
$$10^{-8} \cdot (1.66 \cdot ln(\Delta P'_{\text{valy}}) - 9.97)$$
 (8)

where $\Delta P'_{\text{valy}}$ is the normalized pressure drop with the surface tension.

In the following sections, we evaluate some parametric effects with CHF data obtained with the configuration of BP open in $n_{RP} = 6.25\%$ and preheater inlet valve turn between $n_{\rm ph} = 4$ to 12.5%. These opening valve values were used to ensure greater stability for the flow and allowed the measurement of the highest CHF.

Fig. 7 a Illustration of the preheater inlet (n_{ph}) and bypass (n_{BP}) valves effect on the CHF. Four datasets are included for different bypass (BP) valve opening levels. b Bond number (Bo) is plotted against the normalized pressure drop on the valve, $\Delta P'_{\text{valv}} = d \cdot \Delta P_{\text{valv}} / (2\sigma)$





3.3 Subcooling effect

Generally, the CHF increases with fluid subcooling at the channel inlet. By increasing the liquid subcooling, considerable power input to the fluid is necessary to achieve the critical vapor quality and, consequently, the corresponding CHF.

Figure 8 illustrates the effect of the inlet vapor quality on the CHF. To isolate the inlet vapor quality effect, the comparison is performed based on the critical boiling number (Bo) as a function of the Weber number (We_d), as shown, respectively, in Eqs. 6 and 7. We consider experimental data obtained for the same length-to-diameter ratio (L_h/d = 41.81). According to the figure, the lower inlet vapor quality (-8 to -1.8%) gives higher critical boiling numbers and consequently higher CHF than the higher vapor quality.

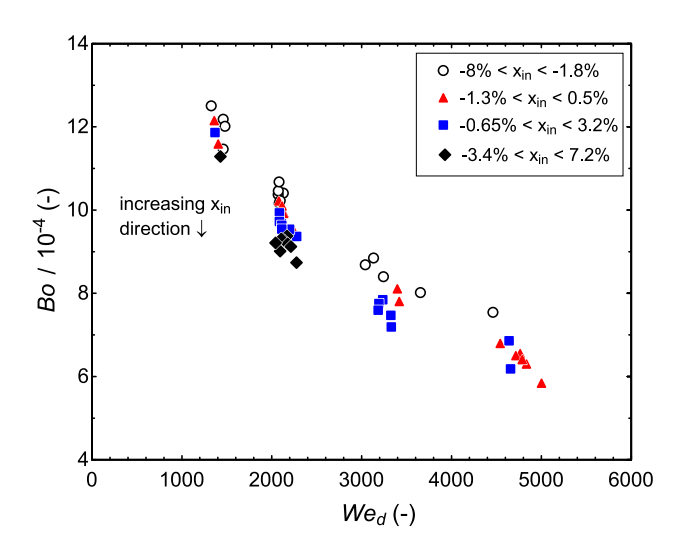
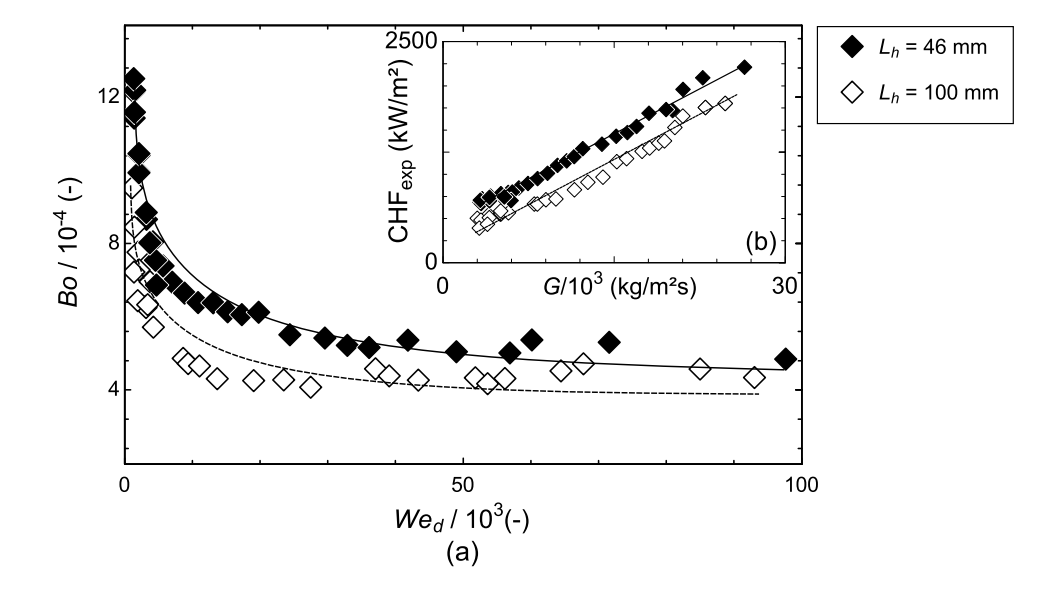
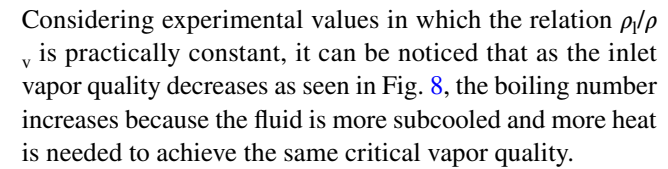


Fig. 8 Relationship between the Bond (Bo) and Weber (We_d) numbers. The Bond number decreases with the inlet vapor quality $(x_{\rm in})$ increment upstream of the test section

Fig. 9 a The Bond number (Bo) is plotted against the Weber number (We_d). The symbols represent the two different lengths of heated sections (L_h) . b The experimentally measured critical heat flux $(\text{CHF}_{\text{exp}})$ corresponding to all evaluated mass velocities (G) in the experiments





The CHF substantially depends on subcooling for high flow rates, unlike for low flow rates. This is because the critical vapor quality for high flow rates is very low, or even negative, while for low flow rate situations, the CHF occurs for elevated vapor quality ($x_{\rm out} > 50\%$) [27]. The decrease in Bo with We_d is related to the decrease in critical vapor quality as fluid velocity rises. This phenomenon will be explored further in the following section.

3.4 Length effect

Reducing the heated length has an effect similar to increasing the subcooling at the inlet of the channel. In Fig. 9a we plot the Bond number (Bo) and Weber number (We) for two heated lengths, $L_h = 46$ and 100 mm. It is observed that both data fit the curves represented, respectively, as $0.0045~{\rm We}_d^{-0.2}$ and $0.0022~{\rm We}_d^{-0.15}$. Keeping the degree of subcooling constant and reducing the heated length, the CHF increases linearly with the mass velocity G, as shown in Fig. 9b.

This effect results from reducing the heat transfer area, and thus, a higher heat flux is necessary to achieve the same critical vapor quality or outlet enthalpy. The dimensionless energy conservation equation Eq. 9 shows that a reduced heated length would imply an inversely proportional increase of the CHF if the outlet vapor quality remains constant. As discussed in Sect. 3.5, for the mass velocity effect, the critical vapor quality (x_{crit}) is not constant as mass velocity changes. Figure 9 shows that for the same tube with 1.1 mm inside diameter and experimental conditions, changing only the heated length from 100 to 46.0 mm, the CHF increased



in 45.65%. These results show that the critical vapor quality reduces with shorter tube lengths, as noted in previous studies [11]. The reduction in the critical vapor quality can be explained by more intense heterogeneous boiling at the tube wall. A higher heat flux increases the evaporation forces, and momentum changes perpendicular to the wall, reducing the liquid contact with the wall.

$$\frac{\text{CHF}}{G \cdot x_{crit} \cdot h_{\text{lv}}} = \frac{1}{4} \cdot \left(\frac{d}{L_h}\right) \tag{9}$$

3.5 Mass velocity effect

Figure 9a and b also illustrates the effect of mass velocity on the CHF. It is essential to observe that the increase of CHF with mass velocity, for the mass flow rates here evaluated, occurs regardless of fluctuations in the degree of subcooling, saturation temperature and heated length. By increasing the mass velocity, we obtain the maximum CHF achieved in this work (2.212 MW/m²), which is the highest CHF for uniform heating in a single tube ever reported in the literature for R134a, see Table 1.

The linear trend, which defines the increase of CHF with the mass velocity in Fig. 9b, is defined by a slope of $\approx 65G$. This slope can change depending on the inlet subcooling. To illustrate that, in Fig. 10, we use a preheater section to change the inlet vapor quality. The experiments are done in lower values of mass velocity (ranging from 3300 to 6000 kg/m 2 s). With that, we note that the slope of the CHF versus G curve changes from G = 4000 kg/m²s. This indicates a change in the mechanism responsible for the CHF, which is initially related to the dryout of the wall due to liquid absence. For high heat flux, related

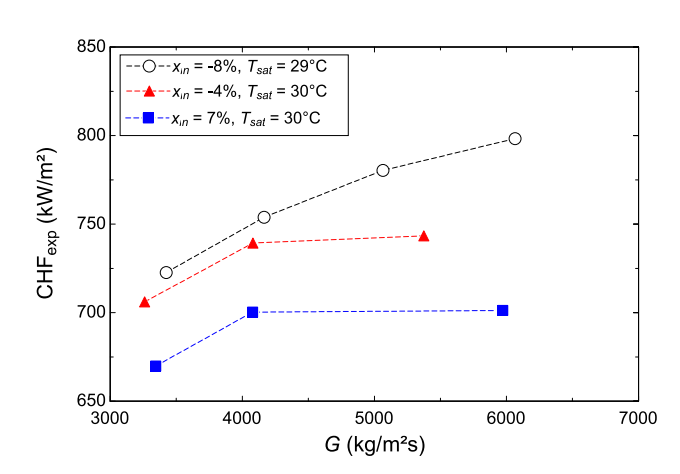


Fig. 10 Effect of mass velocity on CHF in different levels of subcooling. In this scenario $L_h = 46.0 \text{ mm}$ and $L_{ph} = 49.5 \text{ mm}$

to higher flow rates and reduced heated lengths, bubbles nucleate inside liquid film during annular flow [39]. With the increase in nucleation intensity and the possibility of the wall dryout, an inverted annular flow condition is achieved, i.e., the liquid flows in the central region with vapor onto the surface.

The presence of subcooled CHF ($x_{out} \le 0$) mechanism in high flow rates is illustrated in Fig. 11. The data show that the outlet vapor quality $x_{\rm out}$, or critical vapor quality decreases with the We_d in a logarithm curve, Eq. 10:

$$x_{\text{out}} = -0.092 \ln(We_d/1000) + 0.80 \tag{10}$$

High mass velocity flow in a microchannel with inlet subcooled refrigerant resulted in subcooled boiling due to the decrease of the outlet vapor quality and higher CHF values. Mudawar and Bowers [10] illustrate the phenomenon for low and high mass velocity flows characterized by drastically different flow patterns and unique CHF trigger mechanisms. The increment in mass velocities increases the subcooled mechanism in the CHF. Additionally, higher fluid velocities also lead to an increase in the entrainment effect [40].

The experimental data presented in Tab. S1 and analyzed in this section are subsequently utilized to test various correlations. It is worth noting that these correlations are commonly evaluated under low-velocity conditions [41]. However, our dataset with the halogenated fluid R134a, characterized by high mass velocity, proves to be of great importance in testing the limits of these correlations.

3.6 Evaluation of prediction methods

This section compares CHF prediction methods from the literature to the experimental results obtained in this study.

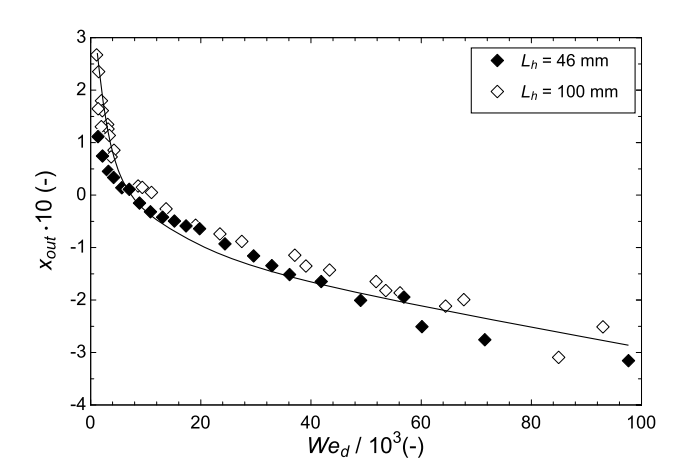


Fig. 11 Effect of mass velocity on outlet vapor quality. The Weber number (We_d) is used to represent the mass velocity



The methods are evaluated according to the mean absolute error (MAE), Eq. 11, and the data portion with deviation from the experimental results below \pm 30%.

$$MAE = \frac{1}{N} \sum_{i=1}^{N} \frac{|CHF_{the_i} - CHF_{exp_i}|}{CHF_{exp_i}} \cdot 100$$
 (11)

where N is the number of points, CHF_{the} is the theoretical value applied in the experimental condition i and CHF_{exp} is the experimental CHF related to this condition.

Table 4 presents the mathematical formulation of the CHF prediction methods as CHF_{the}. The results of the comparisons considering all the experimental data are indicated

 Table 5
 Evaluation of the CHF prediction methods

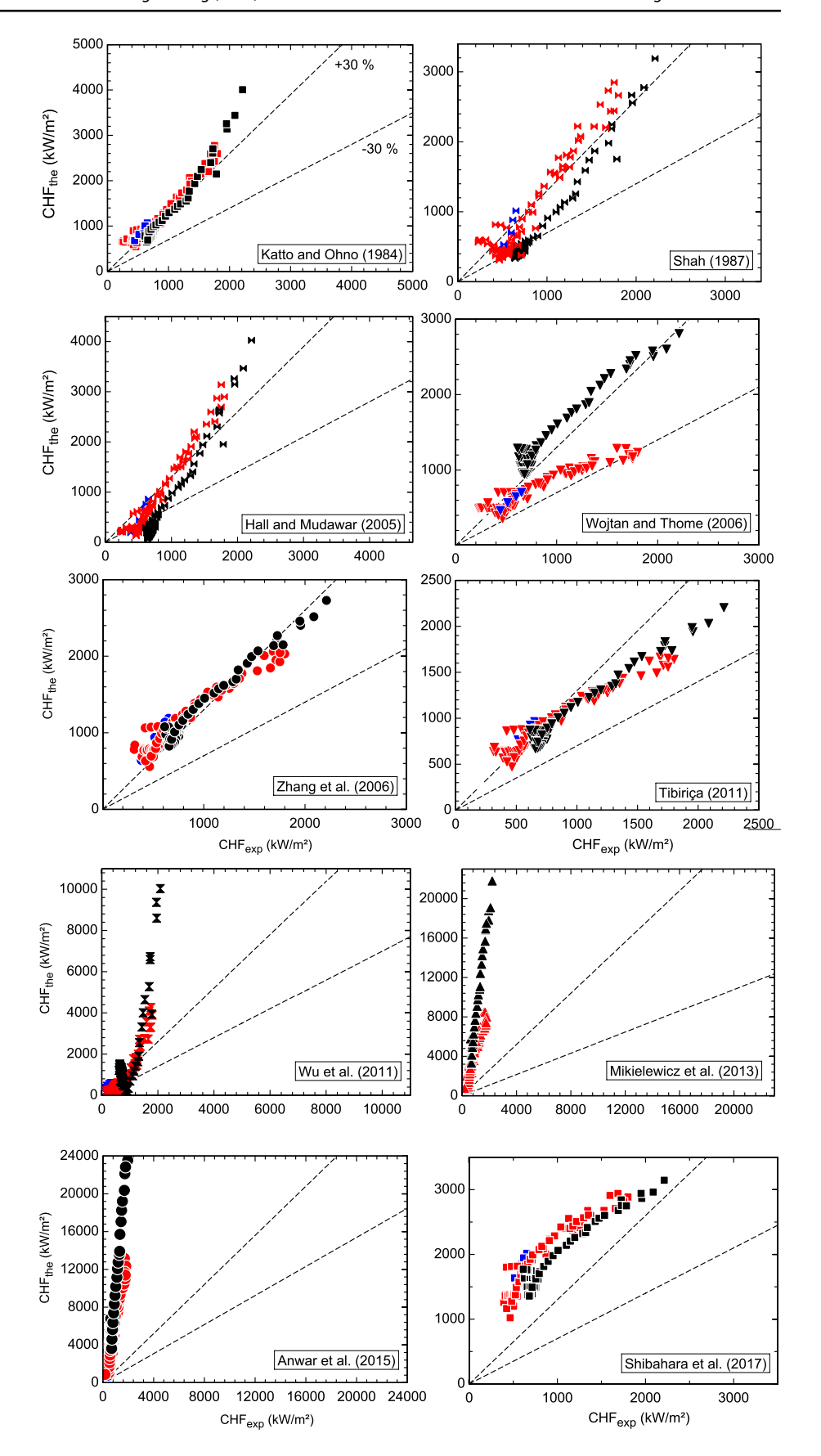
Author(s)	MAE (%)	λ (±30%)
Katto and Ohno [42]	49.25	39.04
Shah [43]	35.99	42.94
Hall and Mudawar [44]	42.48	29.95
Wojtan and Thome [26]	41.03	44.92
Zhang et al. [45]	53.03	18.71
Tibiriçá [46]	30.81	84.26
Wu et al. [47]	64.69	42.94
Mikielewicz et al. [29]	447.71	0
Anwar et al. [30]	590.56	0
Shibahara et al. [48]	153.37	0.59

Table 4 CHF prediction methods from literature

Author(s)	Correlation	
Katto and Ohno [42]	$CHF = q_{co}(1 - Kx_{in})$	(12)
	where q_{co} , $K = f\left[\frac{\rho_v}{\rho_l}, \frac{\sigma \rho_l}{G^2 L_h}, \frac{L_h}{d}\right]$	
Shah [43]	$\frac{\text{CHF}}{Gh_{\text{lv}}} = 0.124 \left(\frac{L_h}{d}\right)^{0.89} \left(\frac{10^4}{Y}\right)^n \left(1 - x_{\text{in}}\right)$	(13)
	where $Y = \text{Pe Fe}^{0.4} (\mu L_{\text{h}} / \mu_{\text{v}})^{0.6}$,	
	$Pe = GdC_{\rm pl}/k_{\rm l}, F_{\rm E} = 1.54 - 0.032 \left(\frac{L_h}{d}\right)$	
Hall and Mudawar [44]	$\frac{\text{CHF}}{Gh_{\text{lv}}} = \frac{C_1 W e^{C_2} \left(\rho_1 / \rho_v\right)^{C_3} \left[1 - C_4 \left(\rho_1 / \rho_v\right)^{C_5} x_{\text{in}}\right]}{1 + 4C_1 C_4 W e^{C_2} \left(\frac{\rho_1}{\rho_v}\right)^{C_3 + C_5} \left(\frac{L_h}{\rho_v}\right)}$	(14)
	Gh_{lv}	
	where $C_1 = 0.0722$, $C_2 = -0.312$,	
	$C_3 = -0.644, \ C_4 = 0.900, \ C_5 = 0.724$	
Wojtan and Thome [26]	$\frac{\text{CHF}}{Gh_{\text{lv}}} = 0.437 \left(\frac{\rho_{\text{v}}}{\rho_{\text{l}}}\right)^{0.073} We^{-0.24} \left(\frac{L_{h}}{d}\right)^{-0.72}$	(15)
Zhang et al. [45]	$\frac{\text{CHF}}{Gh_{\text{lv}}} = 0.0352 \Big[We + 0.0119 \big(L_h/d \big)^{2.31} \big(\rho_{\text{v}}/\rho_{\text{l}} \big)^{0.361} \Big]^{-0.295}$	(16)
	$\times (L_h/d)^{-0.311} \Big[2.05 (\rho_{\rm v}/\rho_{\rm l})^{0.170} - x_{\rm in} \Big]$	
Tibiriçá [46]	$\frac{\text{CHF}}{Gh_{\text{lv}}} = 0.02843 \left(\frac{G^2 d}{\sigma \rho_l} + 0.0119 \left(\frac{L_{\text{h}}}{d} \right)^{2.138} \left(\frac{\rho_{\text{v}}}{\rho_1} \right)^{0.529} \right)^{-0.295}$	(17)
	$\times \left(\frac{\mathrm{L_h}}{\mathrm{d}}\right)^{-0.311} \left(2.05 \left(\frac{\rho_{\mathrm{v}}}{\rho_{\mathrm{l}}}\right)^{0.17} - \mathrm{x_{\mathrm{in}}}\right)$	
Wu et al. [47]	$\frac{\text{CHF}}{Gh_{\text{lv}}} = 0.62 \left(\frac{L_h}{d}\right)^{-1.19} x_{\text{out}}^{0.817}$	(18)
Mikielewicz et al. [29]	$\frac{\text{CHF}}{Gh_{\text{lv}}} = 0.62 \left(\frac{\rho_{\text{v}}}{\rho_{l}}\right)^{-0.02} (We)^{-0.05} \left(\frac{L_{h}}{d}\right)^{-1.17}$	(19)
Anwar et al. [30]	$\frac{\text{CHF}}{Gh_{\text{lv}}} = 0.27 \left(\frac{d}{L_h}\right)$	(20)
Shibahara et al. [48]	$\frac{\text{CHF}}{Gh_{\text{lv}}} = 0.149 \left(\frac{\rho_l}{\rho_v}\right)^{-0.47} D^{*-0.1} W e^{-0.3}$	(21)
	$\times \left(\frac{L_h}{d}\right)^{-0.1} Sp^{0.14}, Sp = \frac{\rho_l c_{pl} \Delta T_{sub,o}}{\rho_{\nu} h_{\text{lv}}}$	



Fig. 12 Comparison between CHF prediction methods from the literature and the experimental data of this work. The blue symbol indicates data for $d = 1.0 \text{ mm} \text{ and } L_h = 100 \text{ mm},$ while red and black symbols indicate d = 1.1 mm for $L_h =$ 100 mm and 46.0 mm, respectively. The dashed line in each graph represents the $\pm 30\%$ error band





in Table 5. At the same time, Fig. 12 shows graphically the dispersion of the experimental data with the correlations.

Considering the values of Table 5, five correlations had MAE lower than 50%, [26, 43, 44, 46, 49], but only the correlation of Tibiriçá [46] had more than 70% of the data within the \pm 30% band. The correlations [26, 43, 49] are widely used for predicting critical heat flux, especially for single channel configuration, as they were developed from a large fluid database, conventional channels and under wide operating conditions. Even though the correlation of Hall and Mudawar [44] is mostly indicated for water, it was validated with data covering a wide range of conditions to the critical point and mass velocity from 1500 to 134000 kg/m²s.

Some correlations considerably overpredicted the CHF values [29, 30, 48]. Despite the fact the correlations of Anwar et al. [30] and Mikielewicz et al. [29] considered R134a and had diameters and heated microchannel lengths close to the used in this study, the authors used lower mass flow rates and saturated CHF. Shibahara et al. [48] also had similar geometry, high flow rate values and subcooled CHF but indicated the utilization only for water. The correlations evaluation at the high mass flow conditions of this study presented results that considerably overestimate the CHF, showing that there are important effects to be incorporated in the models and correlations for halogenated fluids and high mass velocities. At high mass velocities inside microchannels, heat fluxes are much more intense, leading to a strong bubble nucleation process in a confined environment. This intense confined bubble growth promotes forces that develop an inverted annular flow, where liquid phase flows in the core of the tube surrounded by the vapor phase. Additionally, backflow forces arise, which can trigger thermo-hydraulic instabilities, changing the CHF mechanism compared to lower mass flow velocities.

Based on the performance of previous correlations, a new correlation is proposed in this work by adapting the correlation of Zhang et al.[45]. The new correlation is developed with the experimental database from Tibiriçá et al.[41] in addition to the present study, making it more general. The new coefficients were adjusted and are shown in Eq. 22. The correlation of Zhang et al.[45] was limited to water, while this updated version includes results for the fluids R134a, R12, R113, R123, R236fa, R245fa, R1234ze(E), nitrogen and water for tube diameters from 0.24 to 6.92 mm. The results are shown in Fig. 13, where the experimental data of this work are well predicted. The MAE for the new dataset is 11.6% (λ (\pm 30%) = 94.6%), and for the entire database (Tibiriçá et al.[41] including those from the current study), it is 15.7% (λ (\pm 30%) = 80.6%).

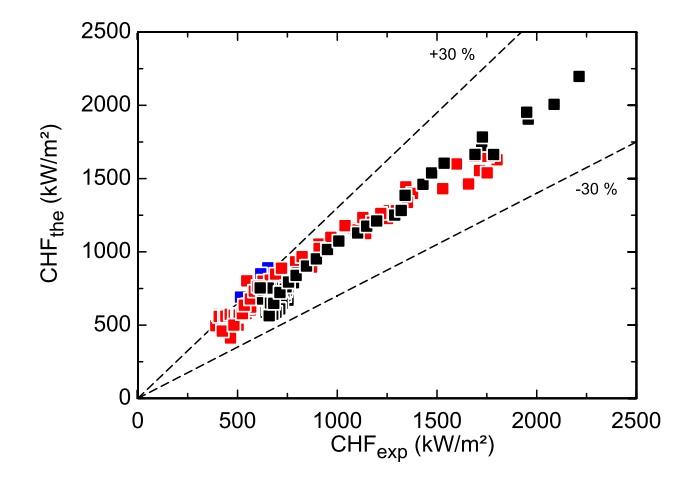


Fig. 13 Comparison between Eq. 22 and the experimental data of this work. The blue symbol indicates data for d=1.0 mm and $L_h=100$ mm, while red and black symbols indicate d=1.1 mm for $L_h=100$ mm and 46.0 mm, respectively. The dashed line in each graph represents the \pm 30% error band

$$\frac{\text{CHF}_{\text{the}}}{Gh_{\text{lv}}} = 0.0284 \left(We + 0.002874 \left(\frac{L_h}{d} \right)^{1.897} \left(\frac{\rho_v}{\rho_l} \right)^{0.0187} \right)^{-0.277} \\
\times \left(\frac{L_h}{d} \right)^{-0.299} \left(1.0683 \left(\frac{\rho_v}{\rho_l} \right)^{0.08279} - x_{\text{in}} \right)$$
(22)

4 Conclusions

New critical heat flux data at high mass velocity for R134a in single circular microchannels were obtained and compared with predictive methods. The analysis has revealed that:

- Based on the literature review, the highest value of CHF for R134a in microchannel was achieved ($q_{\rm chf} = 2.212$ MW/m²) for a mass velocity of 26426 kg/m²s, an internal diameter of 1.1 mm and heated length of 46 mm.
- By increasing the pressure drop of the needled valve installed upstream of the test section from approximately 100 to 500 kPa, the CHF increases by 100%. This effect is related to the reduction of instabilities caused by the strong bubble nucleation process inside microchannels at high heat fluxes.
- The experimental CHF trends agree with the literature, i.e., increases with higher fluid subcooling at the channel inlet, reduced heated length and increased mass velocity for the tubes and flow rates evaluated. The CHF is strongly dependent on fluid inlet subcooling at high mass velocities since the CHF occurs mainly at subcooled conditions or saturated conditions with low vapor quality. This differs from what was observed at low mass veloc-



- ity, where the CHF has a much smaller dependency on the inlet subcooling [50].
- A new correlation is developed, achieving a prediction error of 11.6%.

Supplementary Information The online version contains supplementary material available at https://doi.org/10.1007/s40430-025-05657-z.

Acknowledgements The authors acknowledge the financial support given by FAPESP (The State of São Paulo Research Foundation, Brazil) Contract 2019/11066-9, by Coordination of Superior Level Staff Improvement-Brazil (CAPES)-Financing Code 001, and National Council for Scientific and Technological Development (CNPq), Grant No. 310179/2021-1.

Author contributions RM (RM was with the Heat Transfer Research Group, Department of Mechanical Engineering, São Carlos School of Engineering, University of São Paulo, São Carlos, SP, Brazil. He is now with the Institute of Fluid Dynamics, Helmholtz-Zentrum Dresden Rossendorf, 01328 Dresden, Germany (e-mail: r.maestri@hzdr.de), and was involved in formal analysis, investigation, software, validation, visualization, writing—original draft and writing—review and editing. Cristiano Bigonha Tibiriçá was responsible for conceptualization, formal analysis, funding acquisition, investigation, methodology, project administration, resources, supervision, validation and writing-review and editing.)

Data availability statement Data will be made available on request.

Open Access This article is licensed under a Creative Commons Attribution 4.0 International License, which permits use, sharing, adaptation, distribution and reproduction in any medium or format, as long as you give appropriate credit to the original author(s) and the source, provide a link to the Creative Commons licence, and indicate if changes were made. The images or other third party material in this article are included in the article's Creative Commons licence, unless indicated otherwise in a credit line to the material. If material is not included in the article's Creative Commons licence and your intended use is not permitted by statutory regulation or exceeds the permitted use, you will need to obtain permission directly from the copyright holder. To view a copy of this licence, visit http://creativecommons.org/licenses/by/4.0/.

References

- 1. Song SL, Chang SH (2015) An experimental study on CHF enhancement of wire nets covered surface in R-134a flow boiling under high pressure and high mass flux conditions. Int J Heat Mass Transf 90:761-768. https://doi.org/10.1016/j.ijheatmasstrans
- 2. Hata K, Noda N (2006) Thermal analysis on flat-plate-type divertor based on subcooled flow boiling critical heat flux data against inlet subcooling in short vertical tube. 10(1115/1):2150842
- Radwan A, Ahmed M (2018) Thermal management of concentrator photovoltaic systems using microchannel heat sink with nanofluids. Sol Energy 171:229-246. https://doi.org/10.1016/j.solener. 2018.06.083
- Hong S, Zhang B, Dang C, Hihara E (2020) Development of two-phase flow microchannel heat sink applied to solar-tracking high-concentration photovoltaic thermal hybrid system. Energy 212:118739. https://doi.org/10.1016/j.energy.2020.118739

- 5. Devahdhanush V, Lee S, Mudawar I (2021) Experimental investigation of subcooled flow boiling in annuli with reference to thermal management of ultra-fast electric vehicle charging cables. Int J Heat Mass Transf 172:121176. https://doi.org/10.1016/j.ijhea tmasstransfer.2021.121176
- Collier JG, Thome JR (1994) Convective boiling and condensation
- Becker KM, Hernborg G, Bode M, Eriksson O (1965) Burnout data for flow of boiling water in vertical round ducts, annuli and rod clusters. Technical report, AB Atomenergi
- Griffel J, Bonilla CF (1965) Forced-convection boiling burnout for water in uniformly heated tubular test sections. Nucl Struct Eng 2(1):1–35. https://doi.org/10.1016/0369-5816(65)90133-X
- Celata G, Cumo M, Mariani A (1993) Burnout in highly subcooled water flow boiling in small diameter tubes. Int J Heat Mass Transf 36(5):1269–1285. https://doi.org/10.1016/S0017-9310(05) 80096-1
- 10. Mudawar I, Bowers MB (1999) Ultra-high critical heat flux (CHF) for subcooled water flow boiling-I: CHF data and parametric effects for small diameter tubes. Int J Heat Mass Transf 42(8):1405-1428. https://doi.org/10.1016/S0017-9310(98) 00241-5
- 11. Tibiriçá CB, Czelusniak LE, Ribatski G (2015) Critical heat flux in a 0.38 mm microchannel and actions for suppression of flow boiling instabilities. Exp Therm Fluid Sci 67:48-56. https://doi. org/10.1016/j.expthermflusci.2015.02.020
- 12. Kim JM, Kang SH, Yu DI, Park HS, Moriyama K, Kim MH (2017) Smart surface in flow boiling: spontaneous change of wettability. Int J Heat Mass Transf 105:147–156. https://doi.org/10. 1016/j.ijheatmasstransfer.2016.09.047
- 13. Markal B, Kul B (2023) Effect of a new type staggered pin fin configuration on flow boiling characteristics of micro-heat sinks. J Braz Soc Mech Sci Eng 45(10):552
- Tibiriçá CB, Ribatski G, Thome JR (2012) Flow boiling characteristics for R1234ze (E) in 1.0 and 2.2 mm circular channels. J Heat Transf. https://doi.org/10.1115/1.4004933
- Nascimento FJ, Moreira TA, Ribatski G (2019) Flow boiling critical heat flux of di-water and nanofluids inside smooth and nanoporous round microchannels. Int J Heat Mass Transf 139:240-253. https://doi.org/10.1016/j.ijheatmasstransfer.2019.05.021
- 16. Kanti PK, Wanatasanappan VV, Sharma P, Said NM, Sharma K (2025) Experimental and machine learning insights on heat transfer and friction factor analysis of novel hybrid nanofluids subjected to constant heat flux at various mixture ratios. Int J Therm Sci 209:109548
- 17. Liu B, Yuan B, Zhou J, Zhao J, Di Marco P, Zhang Y, Wei J, Yang Y (2021) Analysis of the critical heat flux of subcooled flow boiling in microgravity. Exp Therm Fluid Sci 120:110238. https://doi. org/10.1016/j.expthermflusci.2020.110238
- Roldão T, Tibiriçá CB (2024) Critical heat flux, heat transfer and pressure drop at high mass fluxes for R123 in a single microchannel. Int J Heat Mass Transf 222:125143. https://doi.org/10.1016/j. ijheatmasstransfer.2023.125143
- Ambreen T, Niyas H, Kanti P, Ali HM, Park C-W (2022) Experimental investigation on the performance of RT-44HC-nickel foam-based heat sinks for thermal management of electronic gadgets. Int J Heat Mass Transf 188:122591
- Tchanche BF, Pétrissans M, Papadakis G (2014) Heat resources and organic Rankine cycle machines. Renew Sustain Energy Rev 39:1185-1199. https://doi.org/10.1016/j.rser.2014.07.139
- 21. Koomey J, Berard S, Sanchez M, Wong H (2010) Implications of historical trends in the electrical efficiency of computing. IEEE Ann Hist Comput 33(3):46-54. https://doi.org/10.1109/MAHC. 2010.28
- Chowdhury AS, Ehsan MM (2023) A critical overview of working fluids in organic Rankine, supercritical Rankine, and supercritical



- Brayton cycles under various heat grade sources. Int J Thermofluids. https://doi.org/10.1016/j.ijft.2023.100426
- Heredia-Aricapa Y, Belman-Flores J, Mota-Babiloni A, Serrano-Arellano J, García-Pabón JJ (2020) Overview of low GWP mixtures for the replacement of HFC refrigerants: R134a, R404a and R410a. Int J Refrig 111:113–123. https://doi.org/10.1016/j.ijrefrig.2019.11.012
- Heath EA (2017) Amendment to the Montreal protocol on substances that deplete the ozone layer (Kigali amendment). Int Leg Mater 56(1):193–205. https://doi.org/10.1017/ilm.2016.2
- Mauro A, Thome J, Toto D, Vanoli GP (2010) Saturated critical heat flux in a multi-microchannel heat sink fed by a split flow system. Exp Therm Fluid Sci 34(1):81–92. https://doi.org/10.1016/j. expthermflusci.2009.09.005
- Wojtan L, Revellin R, Thome JR (2006) Investigation of saturated critical heat flux in a single, uniformly heated microchannel. Exp Therm Fluid Sci 30(8):765–774. https://doi.org/10.1016/j.expth ermflusci.2006.03.006
- Ali R, Palm B (2011) Dryout characteristics during flow boiling of R134a in vertical circular minichannels. Int J Heat Mass Transf 54(11–12):2434–2445. https://doi.org/10.1016/j.ijheatmasstrans fer.2011.02.018
- Del Col D, Bortolin S (2012) Investigation of dryout during flow boiling in a single microchannel under non-uniform axial heat flux. Int J Therm Sci 57:25–36. https://doi.org/10.1016/j.ijthe rmalsci.2012.01.020
- Mikielewicz D, Wajs J, Gliński M, Zrooga A-BR (2013) Experimental investigation of dryout of SES 36, R134a, R123 and ethanol in vertical small diameter tubes. Exp Therm Fluid Sci 44:556–564. https://doi.org/10.1016/j.expthermflusci.2012.08.018
- 30. Anwar Z, Palm BE, Khodabandeh R (2015) Dryout characteristics of natural and synthetic refrigerants in single vertical minichannels. Exp Therm Fluid Sci 68:257–267. https://doi.org/10.1016/j.expthermflusci.2015.04.016
- 31. Mastrullo R, Mauro A, Thome J, Vanoli GP, Viscito L (2016) Critical heat flux: performance of R1234yf, R1234ze and R134a in an aluminum multi-minichannel heat sink at high saturation temperatures. Int J Therm Sci 106:1–17. https://doi.org/10.1016/j.ijthermalsci.2016.03.011
- Tan L, Chen C, Dong X, Gong Z, Wang M (2017) Experimental study on CHF of R134a flow boiling in a horizontal helicallycoiled tube near the critical pressure. Exp Therm Fluid Sci 82:472–481. https://doi.org/10.1016/j.expthermflusci.2016.12.005
- Dalkılıç AS, Özman C, Sakamatapan K, Wongwises S (2018) Experimental investigation on the flow boiling of R134a in a multi-microchannel heat sink. Int Commun Heat Mass Transf 91:125–137. https://doi.org/10.1016/j.icheatmasstransfer.2017. 12.008
- Kandlikar SG (2010) Scale effects on flow boiling heat transfer in microchannels: a fundamental perspective. Int J Therm Sci 49(7):1073–1085
- 35. Tibiriçá CB, Ribatski G (2015) Flow boiling phenomenological differences between micro-and macroscale channels. Heat Transfer Eng 36(11):937–942
- Roldão TCB, Tibiriçá CB (2025) Experimental local heat transfer coefficient for subcooled flow boiling in a microchannel and new predictive method. Appl Therm Eng 268:125826
- Abernathy R, Powell BD, Colbert DL, Sanders DG, Thompson J Jr (1973) Handbook, uncertainty in gas turbine measurements.

- Technical report, Arnold Engineering Development Center, Arnold AFS, TN
- 38. Moffat RJ (1988) Describing the uncertainties in experimental results. Exp Therm Fluid Sci 1(1):3–17
- Tibiriçá CB, Ribatski G (2014) Flow patterns and bubble departure fundamental characteristics during flow boiling in microscale channels. Exp Therm Fluid Sci 59:152–165. https://doi.org/10.1016/j.expthermflusci.2014.02.017
- Wang G, Kuang B, Zhao Y, Han S, Liu P, Hou J (2024) Parameter study for critical heat flux under external reactor vessel cooling condition based on a mechanism model. Appl Therm Eng 238:121992. https://doi.org/10.1016/j.applthermaleng.2023.121992
- Tibiriçá CB, Rocha DM, Sueth Jr I, Bochio G, Shimizu G, Barbosa MC, Santos Ferreira S (2017) A complete set of simple and optimized correlations for microchannel flow boiling and two-phase flow applications. Appl Therm Eng 126:774

 doi.org/10.1016/j.applthermaleng.2017.07.161
- Katto Y, Ohno H (1984) An improved version of the generalized correlation of critical heat flux for the forced convective boiling in uniformly heated vertical tubes. Int J Heat Mass Transf 27(9):1641–1648. https://doi.org/10.1016/0017-9310(84)90276-X
- 43. Shah MM (1987) Improved general correlation for critical heat flux during upflow in uniformly heated vertical tubes. Int J Heat Fluid Flow 8(4):326–335. https://doi.org/10.1016/0142-727X(87)
- Dd HALL, Mudawar I (2000) Critical heat flux (CHF) for water flow in tubes-II.: subcooled CHF correlations. Int J Heat Mass Transf 43(14):2605–2640. https://doi.org/10.1016/S0017-9310(99)00192-1
- Zhang W, Hibiki T, Mishima K, Mi Y (2006) Correlation of critical heat flux for flow boiling of water in mini-channels. Int J Heat Mass Transf 49(5–6):1058–1072. https://doi.org/10.1016/j.ijheatmasstransfer.2005.09.004
- Tibiriçá CB (2011) Estudo teórico-experimental da transferência de calor e do fluxo crítico durante a ebulição convectiva no interior de microcanais. Ph.D. thesis, Universidade de São Paulo
- Wu Z, Li W, Ye S (2011) Correlations for saturated critical heat flux in microchannels. Int J Heat Mass Transf 54(1–3):379–389. https://doi.org/10.1016/j.ijheatmasstransfer.2010.09.033
- Shibahara M, Fukuda K, Liu Q, Hata K (2017) Correlation of high critical heat flux during flow boiling for water in a small tube at various subcooled conditions. Int Commun Heat Mass Transf 82:74–80. https://doi.org/10.1016/j.icheatmasstransfer.2017.02. 012
- Katto Y (1978) A generalized correlation of critical heat flux for the forced convection boiling in vertical uniformly heated round tubes. Int J Heat Mass Transf 21(12):1527–1542. https://doi.org/ 10.1016/0017-9310(78)90009-1
- Tibiriçá CB, Szczukiewicz S, Ribatski G, Thome JR (2013) Critical heat flux of R134a and R245fa inside small-diameter tubes. Heat Transf Eng 34(5–6):492–499. https://doi.org/10.1080/01457632.2012.722457

Publisher's Note Springer Nature remains neutral with regard to jurisdictional claims in published maps and institutional affiliations.

